JCTC Journal of Chemical Theory and Computation

Theoretical Investigation of Solvent Effects on Glycosylation Reactions: Stereoselectivity Controlled by Preferential Conformations of the Intermediate Oxacarbenium-Counterion Complex

Hiroko Satoh,*[,†,‡] Halvor S. Hansen,[†] Shino Manabe,[§] Wilfred F. van Gunsteren,[†] and Philippe H. Hünenberger*[,†]

Laboratory of Physical Chemistry, Swiss Federal Institute of Technology (ETH), CH-8093 Zürich, Switzerland, National Institute of Informatics, Tokyo 101-8430, Japan, and RIKEN Advanced Science Institute, Saitama 351-0198, Japan

Received March 12, 2010

Abstract: The mechanism of solvent effects on the stereoselectivity of glycosylation reactions is investigated using quantum-mechanical (QM) calculations and molecular dynamics (MD) simulations, considering a methyl-protected glucopyranoside triflate as a glycosyl donor equivalent and the solvents acetonitrile, ether, dioxane, or toluene, as well as gas-phase conditions (vacuum). The QM calculations on oxacarbenium-solvent complexes do not provide support to the usual *solvent-coordination hypothesis*, suggesting that an experimentally observed β-selectivity (α-selectivity) is caused by the preferential coordination of a solvent molecule to the reactive cation on the α-side (β-side) of the anomeric carbon. Instead, explicit-solvent MD simulations of the oxacarbenium-counterion (triflate ion) complex (along with corresponding QM calculations) are compatible with an alternative mechanism, termed here the *conformer and counterion distribution hypothesis*. This new hypothesis suggests that the stereoselectivity is dictated by two interrelated conformational properties of the reactive complex, namely, (1) the conformational preferences of the oxacarbenium pyranose ring, modulating the steric crowding and exposure of the anomeric carbon toward the α or β face, and (2) the preferential coordination of the counterion to the oxacarbenium cation on one side of the anomeric carbon, hindering a nucleophilic attack from this side. For example, in acetonitrile, the calculations suggest a dominant $B_{2,5}$ ring conformation of the cation with preferential coordination of the counterion on the α side, both factors leading to the experimentally observed β selectivity. Conversely, in dioxane, they suggest a dominant $^4H_3$ ring conformation with preferential counterion coordination on the β side, both factors leading to the experimentally observed α selectivity.

1. Introduction

In recent years, the investigation of the nature, structure, and function of carbohydrates present in biological systems has received increased interest, especially in the context of glycoscience and chemical biology.[1,2] A major obstacle in the characterization of biologically relevant carbohydrates is the limited availability of pure and structurally well-defined sugar materials; i.e., sugars are usually found in low concentrations and/or in microheterogeneous forms. So far, synthetic chemistry still represents the main access route to oligosaccharides and glycoconjugates with rigorously defined chemical structures.

One of the cornerstones of carbohydrate synthesis is the glycosylation reaction, which involves a glycosyl donor

* Corresponding authors. E-mail: hsatoh@nii.ac.jp (H.S.); phil@igc.phys.chem.ethz.ch (P.H.H.).
† Swiss Federal Institute of Technology (ETH).
‡ National Institute of Informatics.
§ RIKEN Advanced Science Institute.

10.1021/ct1001347
Published on Web 05/21/2010

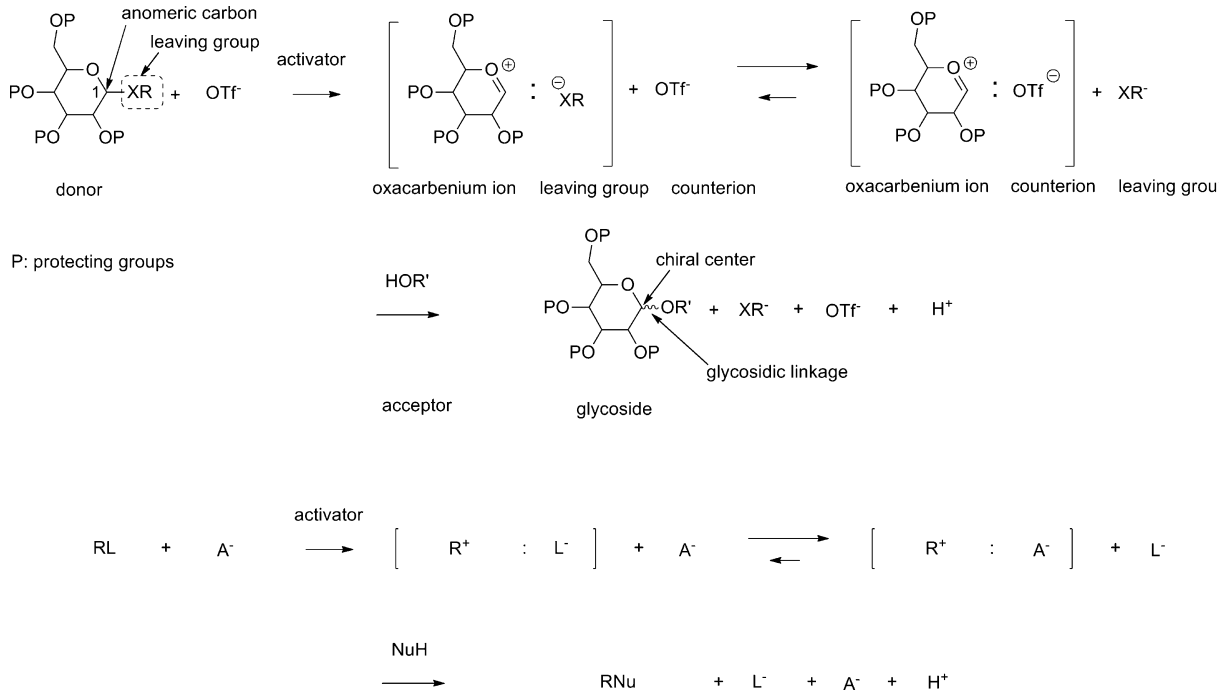

Figure 1. Generic reaction mechanism of a glycosylation reaction, in a solution containing a specific anion. Top: glycosylation involving a protected pyranoside donor, an alcohol acceptor, and triflate anions in solution. Bottom: generalized version, involving an arbitrary glycosyl donor (RL), an arbitrary nucleophile (NuH), and an arbitrary counterion type (A^-).

(electrophile) to be coupled with a glycosyl acceptor (nucleophile) and is promoted by a suitable activator (Figure 1). The exocyclic hydroxyl groups of the donor and of the acceptor that are not involved in the coupling are typically either functionalized or rendered nonreactive by means of protecting groups, while the anomeric carbon (C1) of the donor is functionalized by a leaving group to be substituted by the acceptor. The role of the activator is to assist the departure of this leaving group. Typical leaving groups are imidates, sulfur compounds (thiolates, sulfonates, sulfates), and halogenates. The most common activators are salts of trifluoromethanesulfonate (triflate; OTf^-) and a combination of trifluoromethanesulfonate salts with a chalcogen halide. The reaction creates a glycosidic linkage and induces a new chirality at the anomeric carbon. The products usually consist of a mixture of the two possible stereoisomers, i.e., the α- or β-linkage anomers as defined by IUPAC conventions.[3] Although stereoselective synthetic technologies for oligosaccharides and glycoconjugates have made considerable progress in recent years, including the development of polymer-supported and solid-phase synthesis methodologies,[4−12] a high stereoselectivity is still often difficult to achieve. Since sugar materials that are contaminated with undesirable or indeterminable stereoisomers are less suitable for biological studies, further development of synthetic approaches to control the stereoselectivity of glycosylation reactions is an area of very active research.

Many factors influence the stereoselectivity of a glycosylation reaction, including the choices of the glycosyl donor, leaving group, protecting groups, acceptor, activation system, and solvent, as well as the temperature. Great efforts have been made to gain an understanding of the mechanism of glycosylation reactions and of the relationship between these factors and the resulting stereoselectivity, in particular *via* synthetic experiments[13−39] and theoretical methods.[40−56]

The reaction mechanism for typical pyranosides is generally assumed to be of the SN1 type (Figure 1), with a ratio of products under kinetic (rather than thermodynamic) control and transition barriers of a predominantly enthalpic (rather than entropic) nature. This mechanism involves as a first step the (activator assisted) departure of the leaving group (L^-) and the formation of an oxacarbenium cation intermediate (R^+).[19] This cation benefits from an enhanced stability compared to, e.g., an aliphatic carbocation, generally attributed to the delocalization of the positive charge at the anomeric carbon onto the neighboring ring oxygen atom. For the low to medium polarity organic solvents typically used in glycosylation reactions, a counterion is likely to stay more or less tightly coordinated to this cation. This counterion may be the anionic leaving group L^- or another type of anion A^- present in the reaction medium. In this case, the reactive species will be an oxacarbenium−counterion complex intermediate [R^+; L^-] or [R^+; A^-]. For example, in the common situation where triflate anions are present, the predominant reactive species will be an oxacarbenium−triflate complex intermediate [R^+; OTf^-], which is known as a high reactive glycosylation donor equivalent.[15,17,20,21,23,24,28,32] In a second step, a nucleophile (NuH), typically an alcohol molecule, attacks the anomeric carbon of the intermediate species to form a glycosidic linkage. The nucleophile may attack the oxacarbenium cation from either the α or the β side, resulting in the formation of either of the two corresponding anomers.

The nature of the solvent is known to represent a key factor in the stereoselectivity of glycosylation reactions.[57−67] For glucopyranosides, for example, the 1,2-*cis*-glucoside (α

Table 1. Experimental Results Concerning the Stereoselectivity of Glycosylation Reactions (Figure 1) in Different Solvents (or Solvent Mixtures)[a]

Entry	Donor	Acceptor	Activator	Solvent	α:β
1	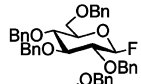	$CH_3OSi(CH_3)_3$	TMSOTf	CH_3CN	16:84
2	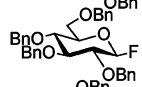	$CH_3OSi(CH_3)_3$	TMSOTf	Et_2O	90:10
3	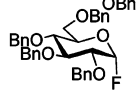	$CH_3OSi(CH_3)_3$	TMSOTf	CH_3CN	22:78
4	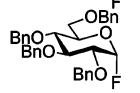	$CH_3OSi(CH_3)_3$	TMSOTf	Et_2O	84:16
5	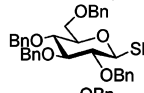	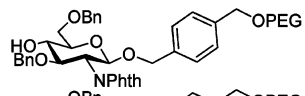	DMTST	CH_2Cl_2-CH_3CN (1:1) % in volume	50:50
6	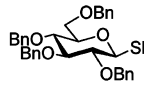	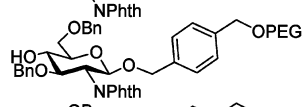	DMTST	CH_2Cl_2-Et_2O (1:1) % in volume	80:20
7	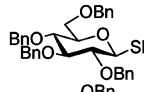	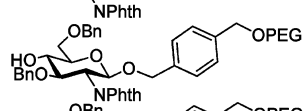	DMTST	toluene	79:21
8	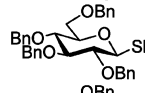	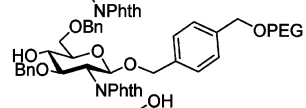	DMTST	CH_2Cl_2	79:21
9	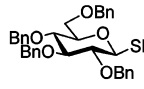	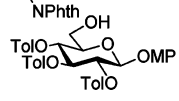	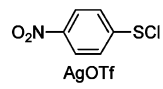	CH_3CN	18:82
10	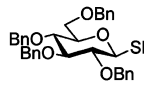	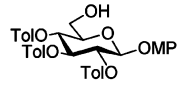	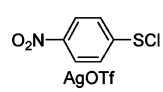	Et_2O	50:50
11	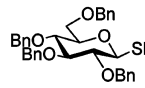	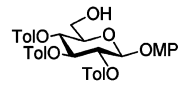	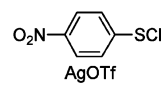	toluene-dioxane (1:1) % in volume	53:47
12	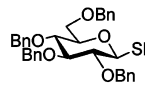	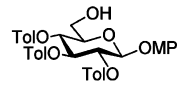	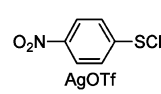	toluene	24:76
13	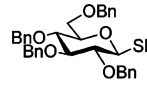	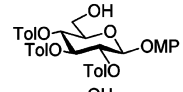	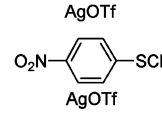	dioxane-CH_3CN (1:1) % in volume	24:76
14	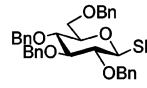	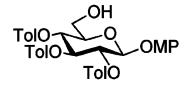	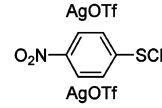	CH_2Cl_2	44:56

Bn = benzyl; Phth = phthaloyl; TMSOTf = trimethylsilyl triflate; PEG = poly(ethylene glycol)methyl ether; Tol = *p*-tolyl; MP = *p*-methoxy phenyl; DMTST = dimethylthiomethylsulfonium triflate

[a] Entries 1−8 are reported from the literature.[61,65] Entries 9−14 correspond to experiments carried out specifically for the present study (see Supporting Information for experimental details).

linkage) is predominantly formed in diethyl ether or in 1,4-dioxane, whereas in acetonitrile, the 1,2-*trans*-glucoside (β linkage) is the major product. The same trend is typically also observed for other pyranosides, namely, that the α-anomer is predominantly formed in ether or dioxane, whereas the β-anomer is predominantly produced in acetonitrile. The solvent effect dominates the stereoselectivity as long as there is no participating effect of neighboring groups (e.g., participation of a 2-acyl protecting group in the donor, predominantly leading to a 1,2-*trans*-glycosidic linkage irrespective of the solvent[35]).

Some examples from the literature[61,64] demonstrating these solvent effects, along with the results of experiments carried out specifically for the present study, are summarized in Table 1 (see also the Supporting Information). Entries 1−4[61] show that the stereoselectivity is essentially insensitive to the anomeric configuration of the glycosyl donor, i.e., to the orientation of the leaving group prior to the reaction, providing support for the general assumption of a SN1 type glycosylation mechanism. These reactions also evidence a clear β-selectivity in acetonitrile and α-selectivity in ether. Entries 5−8[64] correspond to reactions on a poly(ethylene glycol)methyl ether (PEG) polymer support. Here, the α-stereoselectivity observed for an ether/dichloromethane mixture does not differ significantly from that found in solvents usually having little influence on the stereoselectivity (toluene and dichloromethane). However, the acetonitrile/dichloromethane mixture presents a higher proportion of the

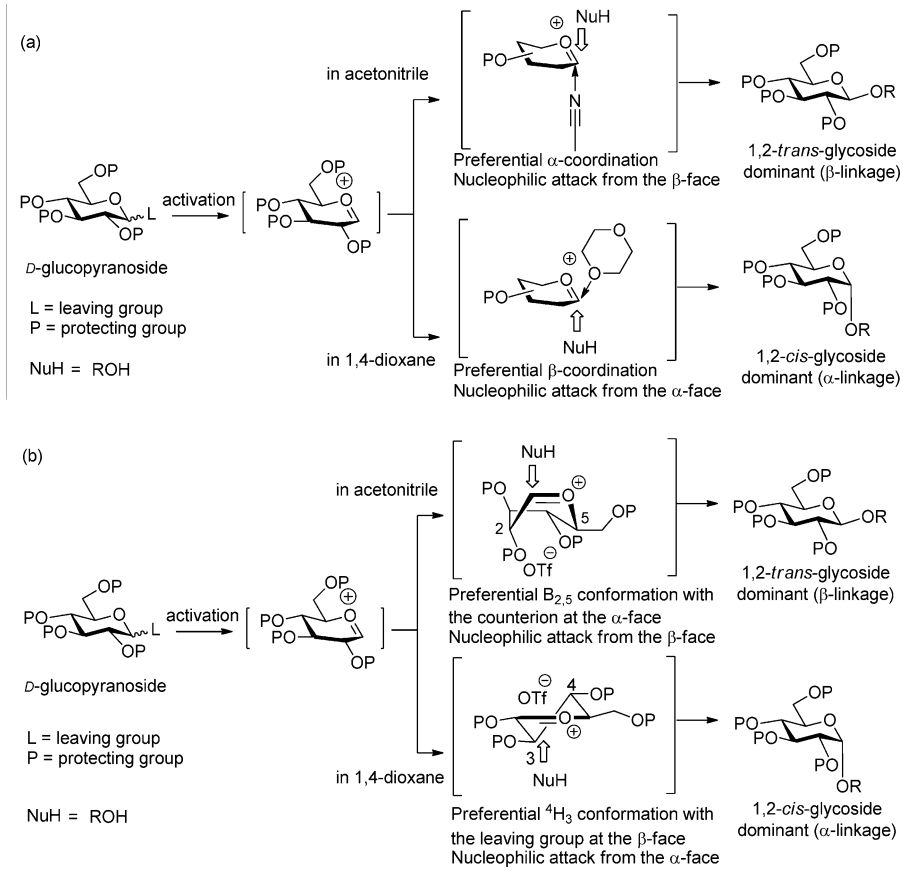

Figure 2. Two alternative hypotheses concerning solvent effects in glycosylation reactions: (a) Commonly formulated hypothesis, referred to here as the *solvent coordination hypothesis*; (b) alternative hypothesis formulated on the basis of the present study, referred to here as the *conformer and counterion distribution hypothesis*. A glucopyranoside donor in the solvents acetonitrile and 1,4-dioxane and in the presence of a triflate counterion are selected here to illustrate how the two hypotheses account for the experimentally observed stereoselectivity.

β-product, albeit no net β-stereoselectivity. Finally, entries 9−14 (experiments carried out for the present study) evidence a clear β-stereoselectivity in acetonitrile and in an acetonitrile/dioxane mixture (as well as in toluene). The proportion of the α product is higher in ether and in a dioxane/toluene mixture (as well as in dichloromethane), although no net α-stereoselectivity is observed. Bearing in mind that the stereoselectivity of glycosylation reactions is affected by many other factors (besides solvent effects), the results presented in Table 1, along with those of other studies,[57−67] suggest a general trend toward β-selectivity in acetonitrile, a general trend toward α-selectivity in ether and dioxane, and little (or nonsystematic) selectivity trends in dichloromethane and toluene. Note, however, that when very reactive donors or high temperatures are considered, the glycosylation reaction may become diffusion-controlled, in which case the stereoselectivity may be partly compromised and solvent effects more complicated.[37]

A commonly formulated hypothesis for the mechanism of solvent effects on glycosylation reactions is that a solvent molecule forms a coordination bond with the anomeric carbon of the oxacarbenium ion, preferentially on one side of the ring, thereby blocking the attack by the nucleophile from the same side (Figure 2a).[18] This interpretation will be referred to here as the *solvent coordination hypothesis*. According to this hypothesis, the predominance of the β product (1,2-*trans* glycoside) in acetonitrile would result from the presence of an acetonitrile molecule preferentially coordinated to the anomeric carbon of the oxacarbenium cation on the α side of the ring. Conversely, the predominance of the α product (1,2-*cis* glycosyde) in ether or dioxane would result from the presence of a solvent molecule preferentially coordinated to the β side. The suggestion that acetonitrile preferentially coordinates to the cation from the α side is apparently supported by experimental investigations of nitrium intermediates in glycosylation reactions.[62] However, these mechanistic studies do not take into account the conformational dynamics of the oxacarbenium cation and the coordination of the counterion. Besides, there is no experimental or theoretical evidence in the literature supporting the suggestion of a preferential coordination of ether or dioxane on the β side.

As will be shown in the present study, quantum-mechanical (QM) calculations on oxacarbenium−solvent interactions in the gas phase and in implicit solvent as well as classical molecular dynamics (MD) simulations of the oxacarbenium intermediate with a triflate counterion (considering a methyl-protected glucopyranoside and the above-mentioned solvents) do not support this hypothesis. Instead, they suggest an alternative mechanism that will be referred to here as the *conformer and counterion distribution hypothesis* (Figure 2b). According to this new hypothesis, the stereoselectivity

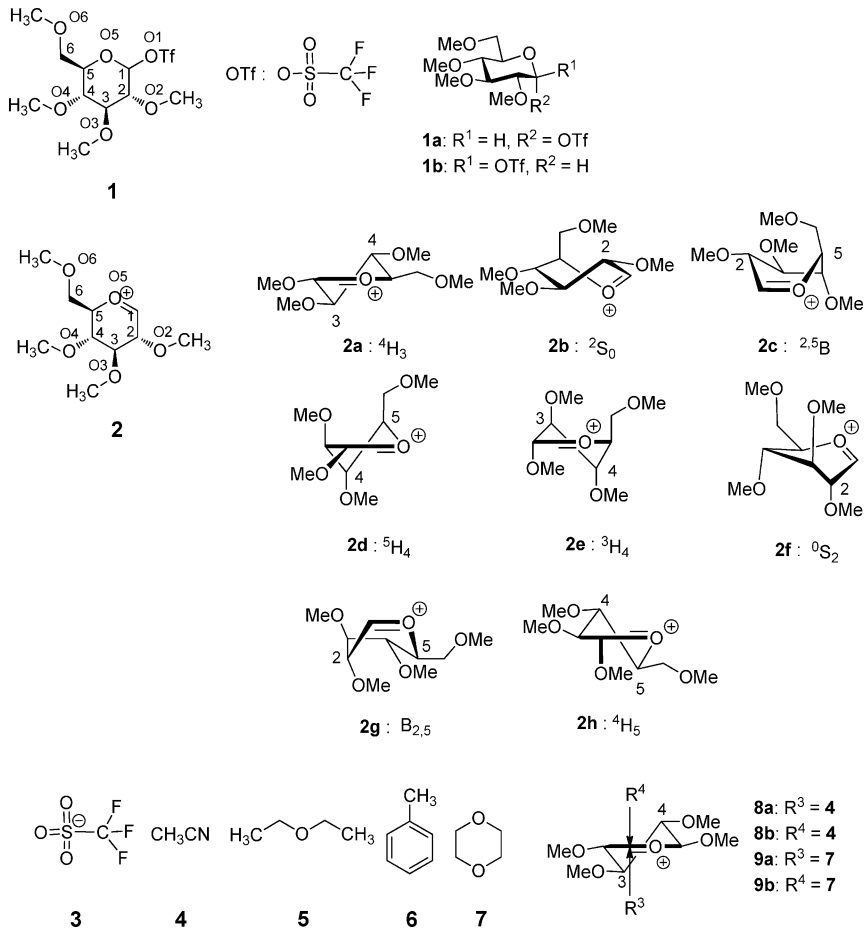

Figure 3. Chemical structures of the species relevant to the present study. 2,3,4,6-tetra-*O*-methyl-D-glucopyranosyl-triflate (**1**), anomeric isomers of **1** (**1a**,**b**), oxacarbenium ion (**2**), representative conformers of the oxacarbenium ion (**2a**−**h**), trifluoromethanesulfonate (triflate) ion (**3**), solvents (**4**, **5**, **6**, **7**), and oxacarbenium-solvent complexes (**8**, **9**), presenting coordination of acetonitrile (**4**) and 1,4-dioxane (**7**) to **2** on the α side (**8a**, **9a**) or on the β side (**8b**, **9b**).

is explained by solvent-induced variations in the ring conformational preferences of the oxacarbenium cation and in the preferential location of the counterion relative to this cation. Taken together, these effects control the side of the anomeric carbon that can be attacked by the nucleophile. In acetonitrile, the oxacarbenium ion preferentially adopts a $B_{2,5}$ boat conformation while the counterion is predominantly located moderately close (on average) to the cation and on the α side. Both effects prevent the acceptor from attacking from the α face and enhance the formation of the β-linked product. In contrast, in ether, in toluene, or in dioxane, the oxacarbenium ion preferentially adopts a $^4H_3$ half-chair conformation, while the counterion is preferentially located very close to the cation and on the β side. Both effects prevent the acceptor from attacking from the β face and enhance the formation of the α-linked product. In the present article, the theoretical evidence supporting this alternative *conformer and counterion distribution hypothesis* as well as the relevance of the alternative *solvent coordination hypothesis* are described and discussed.

The model system selected for the present theoretical investigations (Figure 3) consists of 2,3,4,6-tetra-*O*-methyl-D-glucopyranosyl-triflate (**1**) as a prototypical glycosyl donor, leading upon leaving group departure to a reactive intermediate complex involving a glucopyranosyl oxacarbenium cation (**2**) and a triflate counterion (**3**). Note that, for simplicity (and unlike, e.g., the donors considered in Table 1), the leaving group is chosen here to be the same as the counterion. This system was also investigated in previous QM calculations.[68] The conformational properties of the reactive complex are investigated in the solvents acetonitrile (**4**), diethyl ether (**5**), toluene (**6**), and 1,4-dioxane (**7**), as well as in the gas phase (vacuum).

2. Computational Methods

Quantum Mechanical Calculations. The QM calculations on the reference structures of compounds **1**−**7** and of the oxacarbenium−solvent complexes **8**−**9**, as well as on trajectory structures obtained *via* MD simulations (see further below), were all carried out using density functional theory at the B3LYP/6-31G(d,p) level[69,70] in the electronic ground state using the Gaussian 03 program.[71] The calculations on the reference structures **1**−**9** were performed both in the gas phase (conditions assumed representative for a low polarity solvent such as toluene, dioxane, or ether) and in an implicit solvent (IEF-PCM approach, Integral-Equation Formation−Polarizable Continuum Model[72]) for acetonitrile by using the default parameter of Gaussian 03 for this solvent (dielectric permittivity $\varepsilon = 35.688$). Similarly, the trajectory structures obtained *via* MD simulations in dioxane were analyzed in the gas phase, while those obtained *via* MD

simulations in acetonitrile were investigated using the IEF-PCM approach.

The reference structures of **1**−**7** were generated *via* full geometry optimization in the gas phase for the anomeric isomers of 2,3,4,6-tetra-*O*-methyl-D-glucopyranosyl-triflate (α-anomer **1a** and β-anomer **1b**), initiated from an ideal $^4C_1$ conformation. The energy of **1b** was found to be 28.8 kJ mol^{-1} higher than that of **1a**, as expected from the influence of the anomeric effect.[18,73] The C1−O1 bond lengths in the optimized structures **1a** and **1b** were 0.143 and 0.147 nm, respectively. The energy profile associated with the departure of the triflate anion (**3**) was then calculated by constrained geometry optimization, starting from the optimized structures **1a** and **1b** and progressively elongating the C1−O1 bond from 0.150 to 0.500 nm in steps of 0.005 nm. Removal of the triflate anion (**3**) from the two configurations at maximal elongation led to a unique structure for the oxacarbenium ion (**2**), presenting a $^4H_3$ half-chair conformation (**2a**), in agreement with independent findings.[68] The reference structures of the triflate anion (**3**), as well as of acetonitrile (**4**), diethyl ether (**5**), toluene (**6**), and 1,4-dioxane (**7**) were constructed using the builder function of GaussView[73] followed by full geometry optimization. The reference structures of the corresponding oxacarbenium−solvent complexes (**8a**, **8b**, **9a**, **9b**) were also constructed using GaussView to attach the geometry optimized solvent molecule to the α or β side of the anomeric carbon of **2a**, followed by full geometry optimization.

Finally, a number of trajectory structures corresponding to the most relevant ring conformations observed during the 100 ns MD simulations of **2** with **3** in solution (see below) were further investigated at the QM level. For these calculations, geometry optimization of the intermediate complex was performed with a constraint on the C1−S distance, r, to the peak value of the radial distribution function $P(r)$ obtained from the corresponding MD simulation.

Molecular Dynamics Simulations. The explicit-solvent MD simulations were carried out using the GROMOS simulation program[75] together with the 53A6 force field,[76,77] including recently reoptimized parameters for hexopyranose-based carbohydrates.[78−82] Additional parameters required for the description of the oxacarbenium cation were inferred on the basis of the 53A6 glucose molecule (Lennard-Jones and torsional parameters), along with atomic partial charges derived from an electrostatic potential fit based on the QM results. All force-field parameters used in the present study are reported as Supporting Information. The simulations involved an oxacarbenium cation with a triflate counterion in either acetonitrile, ether, toluene, or dioxane. Independent simulations of the pure solvents were performed for the determination of the corresponding dielectric permittivity values.

For the simulations of the solvated oxacarbenium−counterion complexes, the structures of **2** and **3** optimized at the QM level were solvated by 300 solvent molecules at the experimental (room-temperature) density of the solvent[83] (790, 700, 865, 1040 kg m^{-3} for acetonitrile, ether, toluene, and dioxane, respectively), within cubic computational boxes (edge lengths of about 3.0, 3.7, 6.7, and 3.5 nm, respectively). The pure solvent simulations involved cubic computational boxes containing 1000 solvent molecules at the experimental (room-temperature) density of the solvent.

After energy minimization, initial velocities were assigned from a Maxwell distribution at 300 K, and the systems were equilibrated by 500 ps MD simulation. The production runs were then carried out for a 100 ns (oxacarbenium−counterion complex simulations) or 10 ns (pure solvent simulations) duration. The equations of motion were integrated using a 2 fs time step. The simulations were performed at constant temperature (300 K) and pressure (1 atm) under periodic boundary conditions. The temperature was maintained close to its reference value by weak coupling to a heat bath[84] with a relaxation time of 0.1 ps. The pressure was maintained close to its reference value by weak coupling to a pressure bath[84] (isotropic pressure scaling) with a relaxation time of 0.5 ps and an isothermal compressibility of 0.0004575 (kJ mol^{-1}nm^{-3})$^{-1}$. The center of mass motion was removed every 500 steps. The SHAKE algorithm[84] was applied to constrain the lengths of all covalent bonds and the full rigidity of the solvent molecules. The nonbonded interactions were calculated using a twin-range cutoff scheme,[75,86] with short- and long-range cutoff distances set to 0.8 and 1.4 nm, respectively, and an update frequency of five time steps for the update of the short-range pairlist and intermediate-range interactions. A reaction-field correction was applied to approximately account for the mean effect of electrostatic interactions beyond the long-range cutoff distance. The reaction-field permittivity was set to the corresponding experimental (room temperature) dielectric permittivity of the solvent (38.8, 4.2, 2.4, and 2.2 for acetonitrile,[84] ether,[84] toluene,[87] and dioxane,[88] respectively). Simulations of **2** with **3** in a vacuum at constant temperature (300 K) were also performed for comparison.

The trajectory analyses were performed using the tools of the GROMOS++ software package,[75] as well as several scripts developed for this study. For the oxacarbenium−counterion complex simulations, the conformations of **2** were categorized into eight representative types of conformations of the oxacarbenium ion (Figure 3), namely, $^4H_3$ (**2a**), $^2S_0$ (**2b**), $^{2,5}B$ (**2c**), $^5H_4$ (**2d**), $^3H_4$ (**2e**), $^0S_2$ (**2f**), $B_{2,5}$ (**2g**), and $^4H_5$ (**2h**). These conformations were defined in terms of the torsional angles $\gamma_1-\gamma_5$ around five of the six bonds in the pyranose ring, as detailed in Table 2. The selected dihedral angle ranges were slightly adapted from previous definitions,[45,89] so as to permit the attribution of all sampled configurations to one of the recognized ring conformations. The positioning of the triflate anion (**3**) relative to the oxacarbenium cation was characterized by the spherical coordinates r, θ, and φ describing the direction of the S−C1 vector relative to the local plane of the pyranose ring at C1, as detailed in Figure 4.

For the pure solvent simulations, the permittivity was calculated from the fluctuations of the box dipole moment.

3. Results and Discussion

QM Calculations on Oxacarbenium-solvent Complexes. The optimized geometries of the oxacarbenium−solvent complexes **8a**, **8b**, **9a**, and **9b** (Figure 3) are shown in Figure

Table 2. Definition of the Dihedral Angles and Corresponding Ranges Used to Assign the Different Ring Conformations of the Oxacarbenium Cation (Figure 3), Namely, $^4H_3$ (**2a**), $^2S_0$ (**2b**), $^{2,5}B$ (**2c**), $^5H_4$ (**2d**), $^3H_4$ (**2e**), $^0S_2$ (**2f**), $B_{2,5}$ (**2g**), and $^4H_5$ (**2h**)

	γ_1 C5−O5−C1−C2 [deg]	γ_2 O5−C1−C2−C3 [deg]	γ_3 C1−C2−C3−C4 [deg]	γ_4 C2−C3−C4−C5 [deg]	γ_5 C3−C4−C5−O5 [deg]
2a	0 ± 60	0 ± 80	310 ± 30	50 ± 30	310 ± 30
2b	0 ± 60	0 ± 80	310 ± 30	50 ± 30	0 ± 20
2c	0 ± 60	0 ± 80	310 ± 30	0 ± 20	50 ± 30
2d	0 ± 60	0 ± 80	359 ± 19	310 ± 30	50 ± 30
2e	0 ± 60	0 ± 80	49 ± 31	310 ± 30	50 ± 30
2f	0 ± 60	0 ± 80	49 ± 31	310 ± 30	350 ± 30
2g	0 ± 60	0 ± 80	49 ± 31	5 ± 25	320 ± 40
2h	0 ± 60	0 ± 80	359 ± 19	49 ± 31	320 ± 40

5. The potential energy of the β complex (**8b**) is found to be slightly lower than that of the α complex (**8a**) for acetonitrile (by 0.9 kJ mol^{-1} using the IEF-PCM solvation model; 4.23 kJ mol^{-1} in the gas phase), while the potential energy of the α complex (**9a**) is found to be much lower than that of the β complex (**9b**) for dioxane (gas phase calculation). The above observations are clearly at odds with the *solvent coordination hypothesis* (Figure 2a). This hypothesis would imply a preferential coordination of acetonitrile on the α side (favoring a nucleophilic attack from the β side and leading to the experimentally observed predominance of the β product) and a preferential coordination of dioxane on the β side (favoring a nucleophilic attack from the α side and leading to the experimentally observed predominance of the α product), i.e., a trend exactly opposite to that suggested by the present QM calculations.

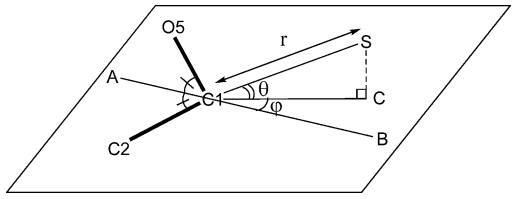

Figure 4. Definition of the spherical coordinates r, θ, and φ used to characterize the positioning of the triflate anion relative to the oxacarbenium cation. These coordinates describe the direction of the C1−S vector relative to the local plane of the pyranose ring at C1. Line AB is the interior bisector of the angle C2−C1−O5. Line SC is perpendicular to the plane C2−C1−O5, C being the intersection point. The distance r corresponds to the length of the C1−S vector. The angle θ corresponds to the angle C−C1−S. The angle φ corresponds to the angle B−C1−C.

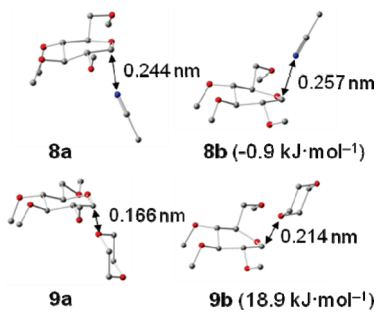

Figure 5. Geometry-optimized structures (QM) of the oxacarbenium-solvent complexes **8** and **9** (Figure 3) involving a coordinated acetonitrile molecule (calculation using an IEF-PCM implicit solvent model) or dioxane molecule (calculation in the gas phase). The distance between the anomeric carbon and the nitrogen atom for **8** or the oxygen atom for **9**, as well as the potential energies of the β complexes (**8b**, **9b**) relative to the α complexes (**8a**, **9a**), are also indicated.

Table 3. Ratios of Ring Conformers (Figure 3) of the Oxacarbenium Ion Observed during the 100 ns MD Simulations of the Oxacarbenium−Counterion Complex in the Different Solvents (As Well As in Vacuum)

	ratio of conformers [%]							
solvent	**2a**	**2b**	**2c**	**2d**	**2e**	**2f**	**2g**	**2h**
4				0.0	36.5	60.7	2.7	0.0
5				0.0	50.1	47.6	2.3	0.0
6			0.0	0.0	70.9	27.7	1.3	0.0
7				0.0	61.4	37.0	1.6	0.0
in vacuum				0.1	68.8	29.6	1.5	0.0

MD Simulations of the Solvated Oxacarbenium−Counterion Complex. As a preliminary calculation, the dielectric permittivities of the solvent models employed for acetonitrile (**4**), ether (**5**), toluene (**6**), and dioxane (**7**) were calculated on the basis of pure solvent MD simulation and were found to be 34.6, 3.5, 1.0, and 1.1, respectively, in good qualitative agreement with the corresponding (room-temperature) experimental values of 35.8, 4.3, 2.4, and 2.2.[83,87,88]

The populations of ring conformers (Figure 3) of the oxacarbenium ion observed during the MD simulations of the oxacarbenium−counterion complexes in the different solvents as well as in vacuum are reported in Table 3. Although all simulations were initiated from the same $^4H_3$ conformation (**2a**), the equilibrium distribution encompasses $^{2,5}B$ (**2c**), $^5H_4$ (**2d**), $^3H_4$ (**2e**), $^0S_2$ (**2f**), $B_{2,5}$ (**2g**), and $^4H_5$ (**2h**) conformers. The $^3H_4$ (**2e**) and the $^0S_2$ (**2f**) conformers are dominant in all simulations, the proportion of the latter increasing with the polarity of the solvent. Thus, for example, the oxacarbenium ion preferentially adopts a $^0S_2$ (**2f**) conformation rather than a $^3H_4$ (**2e**) conformation in acetonitrile (**2e**/**2f** ratio of 36.5:60.7), whereas the opposite is observed in dioxane (**2e**/**2f** ratio of 61.4:37.0). The proportions observed in toluene or in vacuum are close to those found in dioxane, while the proportions observed in ether are intermediate between those found in acetonitrile and dioxane.

The results of the MD simulations concerning the positioning of the counterion relative to the oxacarbenium cation in the different solvents are illustrated graphically in Figures 6 and 7, and summarized numerically in Table 4. The following observations can be made. First, the probability

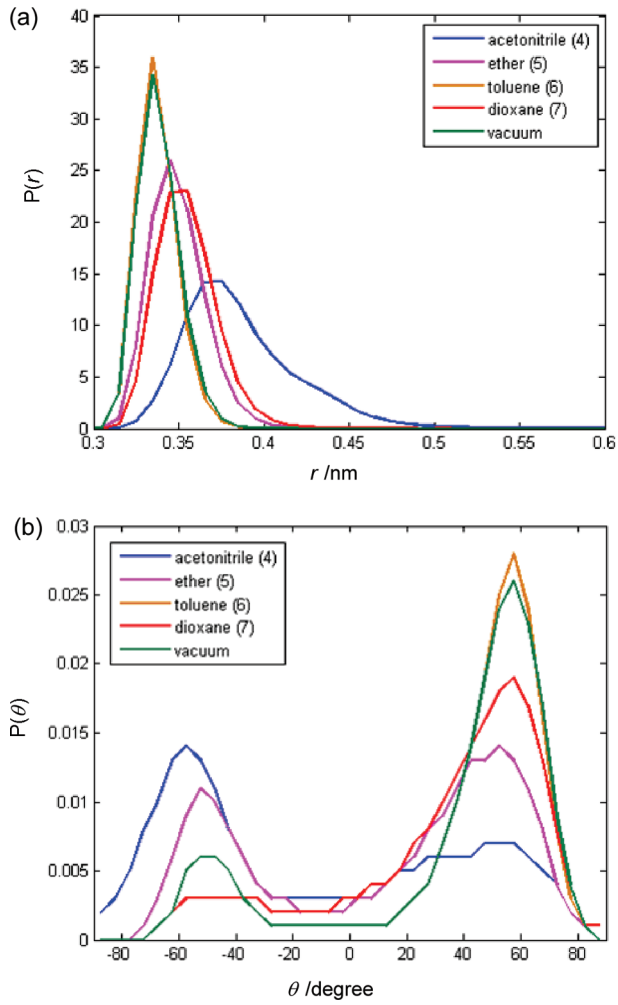

Figure 6. Positioning of the counterion relative to the oxacarbenium cation (Figure 4) observed during the 100 ns MD simulations of the oxacarbenium−counterion complex in the different solvents (as well as in vacuum): (a) distribution $P(r)$ of the distance r; (b) distribution $P(\theta)$ of the angle θ. The $P(\theta)$ functions are normalized according to $\int_{-\pi/2}^{\pi/2} P(\theta) \cos(\theta)\, d\theta = 1$. The probability $P(\theta)$ was also calculated for acetonitrile with a cutoff $r \leq 0.375$ nm, the distance value at the peak of $P(r)$, resulting in a nearly identical distribution (not shown).

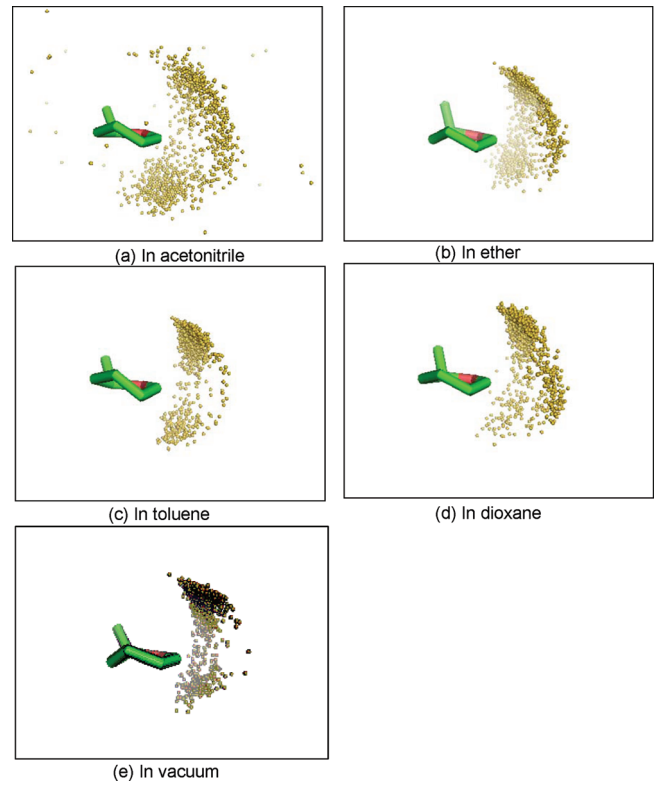

Figure 7. Positioning of the counterion relative to the oxacarbenium cation observed during the 100 ns MD simulations of the oxacarbenium−counterion complex in the different solvents (as well as in vacuum). Successive positions of the triflate S atom along the trajectories are displayed at 100 ps intervals (1000 yellow beads), after superimposition of the trajectory frames onto the initial configuration ($^4H_3$ ring conformation of the oxacarbenium ion) based on all carbon atoms of the cation.

Table 4. Positioning of the Counterion Relative to the Oxacarbenium Cation (Figures 4 and 6) Observed during the 100 ns MD Simulations of the Oxacarbenium−Counterion Complex in the Different Solvents (As Well As in Vacuum)

solvent	$\theta \leq -10°$ (α-side) [%]	$\theta \geq 10°$ (β-side) [%]	$-10° < \theta < 10°$ [%]	$\bar{r}$ [nm]	$\lvert\bar{\varphi}\rvert$ [deg]
4	48.2	41.6	10.2	0.438	53.0
5	33.5	58.9	75.6	0.349	39.8
6	18.4	79.1	2.5	0.338	32.3
7	16.9	74.3	8.8	0.355	35.8
in vacuum	19.2	78.2	2.7	0.338	32.7

distribution $P(r)$ of the C1−S distance r (Figure 6a) tends to become broader, i.e., stretched to larger distances, with an increase of the polarity of the solvent. Second, the probability distribution $P(\theta)$ of the angle θ formed by the C1−S vector and the local ring plane at C1 (Figure 6b) is bimodal, with peaks at about ±55° ($\theta < 0°$, α side; $\theta > 0°$, β side). The population associated with the $\theta = -55°$ peak increases (relative to that associated with the $\theta = +55°$ peak) with increasing polarity of the solvent. In other words, the simulation results show that an increase in the solvent polarity leads to a less tight binding of the triflate counterion to the oxacarbenium cation and to a progressive shift of its preferential positioning from the β to the α side of the ring. This trend is also clearly evident when considering the distributions of the counterion (successive positions of the triflate S atom) along the different trajectories (Figure 7). The correlation between the breadth of the cation−anion distance distribution and the solvent polarity is easily explained in terms of dielectric screening effects (counteracting the direct Coulombic attraction between the two ions). The concomitant shift from a preferential β-side to a preferential α-side coordination upon increasing the solvent polarity is more difficult to rationalize and appears to be correlated with the shift from a dominant $^3H_4$ (**2e**) to a dominant $^0S_2$ (**2f**) conformation (see further below).

As a result of these effects, in acetonitrile, the anion presents a slight preference for the α side ($\theta < -10°$) compared to the β side ($\theta > 10°$), with an α/β ratio of 48.2:41.6 (Table 4). In contrast, it is predominantly found on the β side in ether (33.5:58.9), toluene (18.4:79.1), dioxane (16.9:74.3), and in vacuum (19.2:78.2). The corresponding average

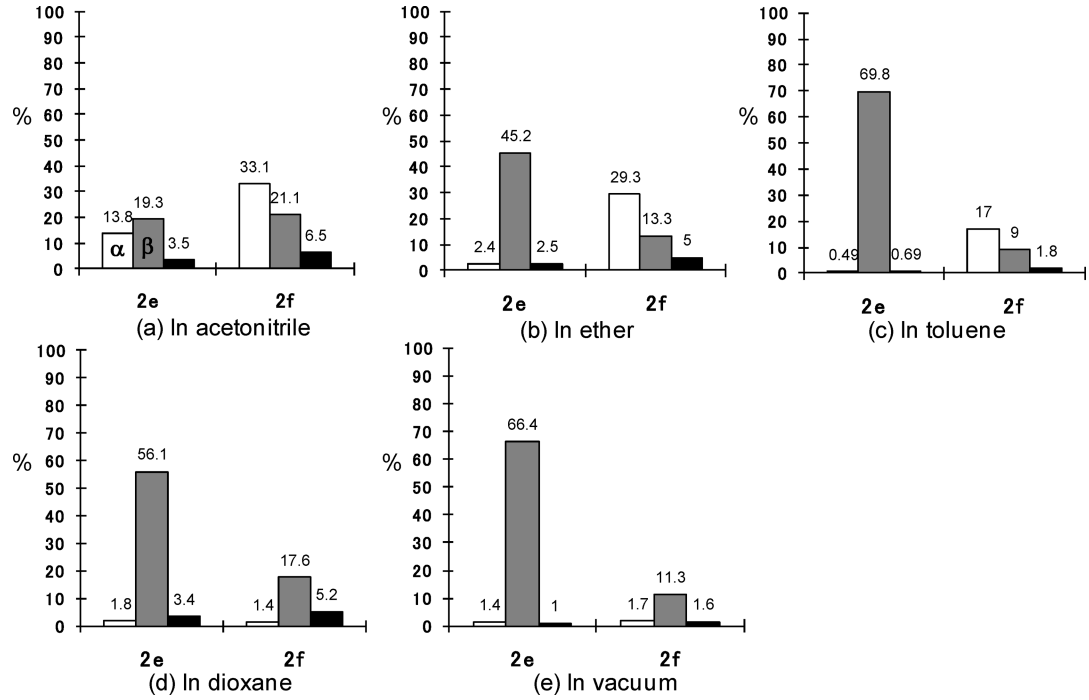

Figure 8. Correlation between the ring conformation of the oxacarbenium cation and the preferential counterion positioning, as observed during the 100 ns MD simulations of the oxacarbenium−counterion complex in the different solvents (as well as in vacuum). The proportions of the sampled configurations corresponding to $^3H_4$ (**2e**) and $^0S_2$ (**2f**) ring conformers, along with α-side ($\theta \leq -10°$; white bars), β-side ($\theta \geq 10°$; gray bars), or in-plane ($-10° < \theta < 10°$; black bars) counterion locations, are reported.

values of r and $|\varphi|$ also show that the triflate ion is more weakly bound to the anomeric carbon in acetonitrile ($\bar{r} =$ 0.438 nm, $|\bar{\varphi}| =$ 53.0°) compared to the other solvents ($\bar{r}$ ranging from 0.338 to 0.355 nm, and $|\bar{\varphi}|$ ranging from 32.3 to 39.8°).

In order to further investigate the correlation between the ring conformation of the oxacarbenium ion and the preferential counterion positioning, the latter positioning was analyzed separately for the configurations presenting $^3H_4$ (**2e**) or $^0S_2$ (**2f**) conformations of the pyranose ring in the different solvents. In acetonitrile (Figure 8a), the dominant configurations involve a $^0S_2$ (**2f**) ring conformation with the counterion on the α side (**2f**-α; 33.1%), while three alternative configurations are nearly equally populated, namely, **2f**-β (21.1%), **2e**-β (19.3%), and **2e**-α (13.8%). In the other solvents (Figure 8b−e), the oxacarbenium ion predominantly adopts a $^3H_4$ conformation (**2e**) with the counterion on the β side (**2e**-β; 45.2%, 69.8%, 56.1%, and 66.4% in ether, toluene, dioxane, and a vacuum, respectively). In dioxane and a vacuum, there is almost no oxacarbenium ion with the counterion at its α side, and the configurations **2e**-β and **2f**-β taken together account for 73.7 and 77.7%, respectively, of the all sampled configurations.

In summary, the MD simulations suggest that, in acetonitrile, the oxacarbenium ion preferentially adopts a $^0S_2$ (**2f**) or, to a lesser extent, a $^3H_4$ (**2e**) conformation, with the counterion loosely bound to the anomeric carbon and distributed nearly equally on the α and β sides (slight α side preference for **2f** and β side preference for **2e**). In contrast, in the solvents of lower polarity, the oxacarbenium ion preferentially adopts a $^3H_4$ (**2e**) conformation with the counterion tightly bound to the anomeric carbon and predominantly on the β side. This β side preference is also observed for the minor $^0S_2$ conformer.

The above observations provide support to the *conformer and counterion distribution hypothesis* (Figure 2b). This hypothesis suggests that, in acetonitrile, the preferential ring conformation ($^0S_2$) and counterion positioning (α side) both favor an attack of the nucleophile from the β side, leading to the experimentally observed predominance of the β product, while in a solvent of lower polarity, the preferential ring conformation ($^3H_4$) and counterion positioning (β side) both favor an attack of the nucleophile from the α side (leading to the experimentally observed predominance of the α product). This is in excellent agreement with the results of the present MD simulations for acetonitrile, ether, and dioxane. Note that this interpretation differs from the previously formulated hypothesis[49] that $^4H_3$ conformers are preferentially α-selective and $^3H_4$ conformers β-selective, indicating that the consideration of the counterion positioning is essential in the theoretical investigation of glycosylation intermediates.

The simulation results are, however, in apparent contradiction with the *conformer and counterion distribution hypothesis* in the case of toluene. For this solvent, the conformational properties of the oxacarbenium−counterion complex are similar to those observed in ether, dioxane, and vacuum. However, synthetic experiments usually observe no or a low stereoselectivity in toluene.[60,61,63−65,67] One possible reason for this discrepancy is that the conformational properties of the oxacarbenium−counterion complex in toluene are influenced by effects that are not

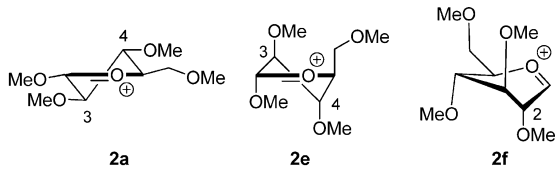

	2a	2e	2f
in acetonitrile	0 kJ·mol^{-1}	-3.6 kJ·mol^{-1}	-1.2 kJ·mol^{-1}
	4.9 Debye	4.2 Debye	4.3 Debye
in vacuum	0 kJ·mol^{-1}	-28.5 kJ·mol^{-1}	-26.2 kJ·mol^{-1}
	3.6 Debye	2.9 Debye	2.9 Debye

Figure 9. Geometry-optimized structures (QM) of the oxacarbenium cation (**2**) in $^4H_3$ (**2a**), $^3H_4$ (**2e**), and $^0S_2$ (**2f**) ring conformations in acetonitrile (calculation using an IEF-PCM implicit solvent model) or in the gas phase (assumed representative for dioxane). The potential energies (relative to **2a**) and the dipole moments (relative to the center of charge) are also indicated.

taken into account appropriately in classical force-field simulations, such as stereoelectronic effects and cation$-\pi$ interactions. Note, however, that a significant (nonsystematic) stereoselectivity may also be observed in this solvent, depending on the donor, acceptor, and activator (e.g., entries 7 and 12 in Table 1, evidencing clear α- and β-stereoselectivities, respectively).

QM Analysis of Selected MD Trajectory Structures. The classical force-field representation employed in the MD simulations takes realistically into account solvation effects but has its shortcomings, including an approximate description of stereoelectronic effects (controlling in particular the relative stabilities of the different ring conformations). For this reason, selected configurations of the oxacarbenium−counterion complex presenting different ring conformations were extracted from the simulations in acetonitrile and dioxane and subjected to a QM analysis, i.e., geometry optimization and energy evaluation. These calculations were performed using the IEF-PCM implicit solvent model (acetonitrile) or in the gas phase (dioxane).

In a first step, configurations of the oxacarbenium ion without the counterion were geometry optimized starting from MD configurations presenting the $^3H_4$ (**2e**) or the $^0S_2$ (**2f**) conformations. This optimization did not result in ring conformational changes (for $^3H_4$, this observation contradicts previous suggestions concerning the stability of this conformer during QM calculations[55]). The final energies and dipole moments, in both acetonitrile and in vacuum (dioxane), are reported in Figure 9 and compared to the corresponding values for the geometry optimized $^4H_3$ conformation (**2a**). The latter conformation is often considered to be the most stable one for a typical oxacarbenium cation[36,89−92] and was used as the starting conformation for the MD simulations. Both of the structures predominantly sampled during the MD simulations (**2e**, **2f**) are about 1−3 and 26−28 kJ mol^{-1} more stable than **2a** in acetonitrile and in vacuum, respectively. The energy ranking of the three structures matches that of the dipole moment magnitudes; i.e., the favored conformations (**2e** and, to a slightly lesser extent, **2f**) are those with the lowest dipole moment. Expectedly, the energy differences are much larger in vacuum (dioxane) compared to acetonitrile, because a polar medium more efficiently stabilizes conformations with a higher dipole moment. The observed trends are in good qualitative agreement with the relationships inferred from the MD simulations between preferential ring conformations and solvent polarity.

In a second step, configurations of the oxacarbenium−counterion complex were geometry optimized starting from MD configurations presenting a $^3H_4$ conformation with the counterion on the α side (**2e**-α) or β side (**2e**-β), or a $^0S_2$ conformation with the counterion or the α side (**2f**-α) or β side (**2f**-β). These optimizations were performed with a constraint on the C1−S distance, set to the peak value of $P(r)$ (Figure 6a) as determined in the MD simulations in acetonitrile (0.38 nm) or in dioxane (0.34 nm). In four cases, the optimization resulted in a conformational change of the ring to either a $^5H_4$ (**2d**), a $B_{2,5}$ (**2g**), or a $^4H_3$ (**2a**) configuration, namely, **2e**-β → **2d**-β, **2f**-α → **2g**-α, and **2f**-β → **2g**-β in acetonitrile and **2f**-β → **2a**-β in vacuum (dioxane). The final energies and dipole moments, in both acetonitrile and vacuum (dioxane), are reported in Table 5 and compared to the relative conformer populations (**2e**-α, **2e**-β, **2f**-α, and **2f**-β) observed in the corresponding MD simulations (Figure 8).

Table 5. Relative Energies Corresponding to Geometry-Optimized Structures (QM) of the Oxacarbenium Cation (**2**) Presenting Different Ring Conformations (Figure 3) and Counterion (**3**) Positioning (α or β) in Acetonitrile (Calculation Using an IEF-PCM Implicit Solvent Model) or in Vacuum (Assumed Representative for Dioxane)[a]

entry no.	starting conformation of **2**	location of **3**	ratio in MD simulations [%]	conformation of **2** in optimized complex	relative energy [kJ mol^{-1}]	dipole moment [Debye]
			in acetonitrile			
1	**2e**	α	13.8	**2e**	0	19.2
2		β	19.3	**2d**	–11.3	15.6
3	**2f**	α	33.1	**2g**	–13.4	17.8
4		β	21.1	**2g**	2.3	17.9
			in vacuum			
5	**2e**	α	0.17	**2e**	0	10.0
6		β	56.1	**2e**	–20.3	9.5
7	**2f**	α	1.4	**2f**	–18.9	10.7
8		β	17.6	**2a**	–28.7	9.7

[a] The energies are given relative to entries 1 (in acetonitrile) or 5 (in vacuum). The corresponding dipole moments (relative to the center of charge) are also reported. The initial ring conformation prior to geometry optimization and the occurrence of this specific configuration in the MD simulations are also indicated.

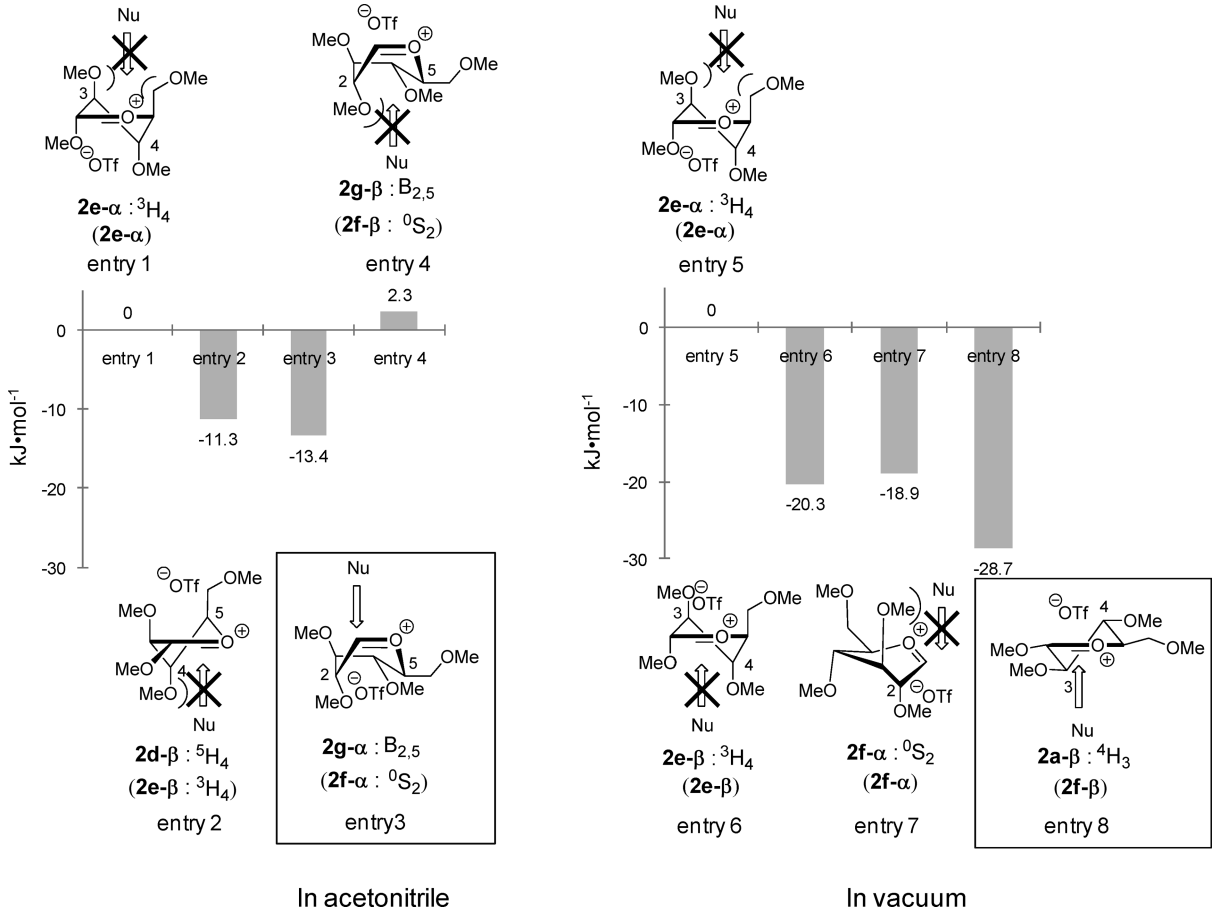

Figure 10. Relative potential energies corresponding to geometry-optimized structures (QM) of the oxacarbenium cation (**2**) presenting different ring conformations and counterion (**3**) positioning (α or β side) in acetonitrile (calculation using an IEF-PCM implicit solvent model) or in vacuum (assumed representative for dioxane). The entry numbers refer to Table 5. The energies are given relative to entries 1 (in acetonitrile) or 5 (in vacuum). The initial ring conformation prior to geometry optimization is indicated between parentheses.

Although the MD simulations and QM calculations suggest slightly different dominant configurations for the reactive oxacarbenium−counterion complex in acetonitrile (**2f**-α and **2g**-α, respectively), these configurations present two common features. First, the coordination of the counterion on the α face blocks a nucleophilic attack from this side. Second, the lack of steric crowding and high exposure of the anomeric carbon toward the β face facilitates a nucleophilic attack from this side (Figure 10). In contrast, **2e**-α, **2d**-β, and **2g**-β are sterically crowded on the face opposite the counterion. These observations are consistent with the experimentally observed predominance of the β-product in acetonitrile. Note that the conformations identified here do not include the $^5S_1$ conformer, which was proposed previously on the basis of QM calculations on the same compound in dichloromethane,[91] this conformation being similar to **2g** except for the pseudoequatorial orientation of C2−O2 bond.

The MD simulations and QM calculations also suggest different dominant configurations for the reactive oxacarbenium−cation complex in dioxane (**2e**-β and **2a**-β, respectively). However these configurations again present two common features. First, the coordination of the counterion on the β face blocks a nucleophilic attack from this side. Second, the lack of steric crowding and high exposure of the anomeric carbon toward the α face facilitates a nucleophilic attack from this side (Figure 10; although the exposure is similar, the steric crowding is slightly higher for **2e**-β compared to **2a**-β). In contrast, **2e**-α and **2f**-α are sterically crowded on the face opposite the counterion. These observations are consistent with the experimentally observed predominance of the α product in dioxane.

The suggestion of a $^4H_3$ conformation with the counterion on the β side (**2a**-β) for the reactive intermediate complex in solvents of low polarity (α-selectivity) is also compatible with the result of glycosylation experiments involving conformationally locked pyranosides functionalized by a *N*-benzyl-2,3-*trans*-oxazolidinone group.[93−96] For these compounds, $^4H_3$ is the only possible conformation of the pyranose ring, and in agreement with the present suggestion, these compounds predominantly lead to the formation of α-linked glycosides.

To our knowledge, the present work is the first study suggesting a key role for the (solvent-modulated) counterion coordination in influencing the stereoselectivity of glycosylation reactions, besides a previously postulated role of this anion as a proton acceptor near the transition state of the reaction.[55]

4. Conclusions

The present study combines QM calculations and explicit-solvent MD simulations to gain a better understanding of solvent effects on the stereoselectivity of glycosylation reactions. To this purpose, a model system consisting of a methyl-protected triflate glucopyranoside in different solvents (acetonitrile, ether, dioxane, toluene, and in vacuum) is considered.

The common assumption concerning solvent effects on the stereoselectivity of glycosylation reactions, *the solvent coordination hypothesis*, suggests that the preferential coordination of a solvent molecule to the reactive oxacarbenium cation on one side of the anomeric carbon (α or β) hinders a nucleophilic attack from this side, thereby favoring the product with the opposite stereochemistry (β or α). The present calculations do not support this hypothesis. For example, an acetonitrile molecule is predicted to preferentially bind on the β side, in disagreement with the experimentally observed α-selectivity in this solvent. Conversely, a dioxane molecule is predicted to preferentially bind on the α side, in disagreement with the experimentally observed α-selectivity.

However, the present calculations support an alternative explanation, termed here the *conformer and counterion distribution hypothesis*. This new hypothesis suggests that the stereoselectivity is dictated by two interrelated conformational properties of the reactive oxacarbenium−counterion complex, namely, (1) the conformational preferences of the oxacarbenium pyranose ring, modulating the steric crowding and exposure of the anomeric carbon toward the α or β face, and (2) the preferential coordination of the counterion to the oxacarbenium cation on one side of the anomeric carbon, hindering a nucleophilic attack from this side. For example, in acetonitrile, the calculations suggest a dominant $^{0}S_{2}$ (MD) or $B_{2,5}$ (QM) ring conformation of the oxacarbenium ion with preferential coordination of the counterion on the α side within the reactive intermediate complex. Both factors render the anomeric carbon most accessible from the β side, in agreement with the experimentally observed β-selectivity in this solvent. Conversely, in dioxane, the calculations suggest a dominant $^{3}H_{4}$ (MD) or $^{4}H_{3}$ (QM) ring conformation with preferential counterion coordination on the β side. Both factors render the anomeric carbon most accessible from the α side, in agreement with the experimentally observed α selectivity in this solvent. The reactive conformations predicted by the QM calculations ($B_{2,5}$ in acetonitrile and $^{4}H_{3}$ in dioxane) are probably more realistic, since these calculations take more appropriately into account the stereoelectronic effects controlling the relative stabilities of the different ring conformations.

In the case of dioxane, the $^{4}H_{3}$ conformation is indeed the one usually considered to be the most stable for typical oxacarbenium cations.[36,90−92] It is also the only possible conformation in the case of conformationally locked pyranosides functionalized by a *N*-benzyl-2,3-*trans*-oxazolidinone group, which predominantly lead to α-linked disaccharides upon glycosylation.[93−96] In the case of acetonitrile, the suggestion of a reactive $B_{2,5}$ conformation has been formulated previously on the basis of experiments on *N*-(tetra-O-acetyl-α-D-glucopyranosyl-4-methyl-pyridinium bromide) in aqueous solution.[97,98] The shift between the former and latter conformations upon increasing the polarity of the solvent may tentatively be attributed to dielectric screening effects, increasingly stabilizing conformers with higher dipole moments.

In summary, the theoretical (and experimental) data discussed in the present study are clearly compatible with the new *conformer and counterion distribution hypothesis* and do not provide support to the more common *solvent coordination hypothesis*. However, mechanistic hypotheses can seldom be formally "proved". They can only be strengthened by accumulation of compatible data and elimination of concurrent hypotheses. In this sense, the present work provides preliminary evidence for a key role of the oxacarbenium conformation and counterion coordination within the reactive complex. Theoretical and experimental work is currently in progress to further refine this new hypothesis.

Acknowledgment. The present calculations were performed on Obelix, a computer cluster of the Competence Center for Computational Chemisty (C^{4}). The authors would like to thank Hans Peter Lüthi, Maria Reif, and the members of the group for computer-aided chemistry (IGC) for their help and for many valuable discussions.

Supporting Information Available: All force-field parameters used in the present study as well as the experimental procedures employed and the ^{1}H NMR and ^{13}C NMR spectral characteristics of the two disaccharides (α- and β-linked) newly synthesized for the present study (entries 9−14 of Table 1) are provided. This information is available free of charge *via* the Internet at http://pubs.acs.org/.

References

(1) Stallforth, P.; Lepenies, B.; Adibekian, A.; Seeberger, P. H. Carbohydrates: A Frontier in Medicinal Chemistry. *J. Med. Chem.* **2009**, *52*, 5561–5577.

(2) Seeberger, P. H. Chemical glycobiology: why now. *Nature Chem. Biol.* **2009**, *5*, 368–372.

(3) The stereoselectivity is often described using relative stereodescriptors to describe the configuration at the anomeric carbon, α and β, instead of the notation 1,2-*cis* and 1,2-*trans*. The α descriptor is used for the case where the OH at the anomeric carbon is on the same side as the OH at the reference atom in the Fischer projection, and the β descriptor is used for the opposite side. In the case of glucopyranosides, the 1,2-*cis* and 1,2-*trans* positions are defined as the α and β configurations for the anomeric carbon, respectively. For more details, see the IUPAC definition at http://www.chem.qmul.ac.uk/iupac/2carb/06n07.html (accessed April 13, 2010).

(4) Manabe, S.; Ito, Y. On-Resin Real-Time Reaction Monitoring of Solid-Phase Oligosaccharide Synthesis. *J. Am. Chem. Soc.* **2002**, *124*, 12638–12639.

(5) Simon, J.; Liu, K.; Schmidt, R. R. Solid-Phase Oligosaccharide Synthesis of a Small Library of *N*-Glycans. *Chem.—Eur. J.* **2006**, *12*, 1274–1290.

(6) Ando, H.; Manabe, S.; Nakahara, Y.; Ito, Y. Tag-Reporter Strategy for Facile Oligosaccharide Synthesis on Polymer Support. *J. Am. Chem. Soc.* **2001**, *123*, 3848–3849.

(7) Ando, H.; Manabe, S.; Nakahara, Y.; Ito, Y. Solid-Phase Capture-Release Strategy Applied to Oligosaccharide Synthesis on a Soluble Polymer Support. *Angew. Chem., Int. Ed.* **2001**, *40*, 4725–4728.

(8) Hanashima, S.; Manabe, S.; Ito, Y. Divergent Synthesis of Sialylated Glycan Chains: Combined Use of Polymer Support, Resin Capture-Release, and Chemoenzymatic Strategies. *Angew. Chem., Int. Ed.* **2005**, *44*, 4218–4224.

(9) Kantchev, E. A. B.; Bader, S. J.; Parquette, J. R. Oligosaccharide Synthesis on a Soluble, Hyperbranched Polymer Support Via Thioglycoside Activation. *Tetrahedron* **2005**, *61*, 8329–8338.

(10) Bauer, J.; Rademann, J. Hydrophobically Assisted Switching Phase Synthesis: The Flexible Combination of Solid-Phase and Solution-Phase Reactions Employed for Oligosaccharide Preparation. *J. Am. Chem. Soc.* **2005**, *127*, 7296–7297.

(11) Fukase, K.; Takashina, M.; Hori, Y.; Tanaka, D.; Tanaka, K.; Kusumoto, S. Oligosaccharide Synthesis by Affinity Separation Based on Molecular Recognition between Podand Ether and Ammonium Ion. *Synlett* **2005**, 2342–2346.

(12) Goto, K.; Miura, T.; Hosaka, D.; Matsumoto, H.; Mizuno, M.; Ishida, H.; Inazu, T. Rapid Oligosaccharide Synthesis on a Fluorous Support. *Tetrahedron* **2004**, *60*, 8845–8854.

(13) Barresi, F.; Hindsgaul, O. In *Modern Methods in Carbohydrate Synthesis*; Khan, S. H., O'Neil, R. A., Eds.; Harwood Academic Publishers: Amsterdam, 1996; pp 251−276.

(14) Miliković, M.; Yeagley, D.; Deslongchamps, P.; Dory, Y. L. Experimental and Theoretical Evidence of Through-Space Electrostatic Stabilization of the Incipient Oxocarbenium Ion by an Axially Oriented Electronegative Substituent During Glycopyranoside Acetolysis. *J. Org. Chem.* **1997**, *62*, 7597–7604.

(15) Crich, D.; Sun, S. Are Glycosyl Triflates Intermediates in the Sulfoxide Glycosylation Method? A Chemical and ^{1}H, ^{13}C, and ^{19}F NMR Spectroscopic Investigation. *J. Am. Chem. Soc.* **1997**, *119*, 11217–11223.

(16) Pozsgay, V. In *Carbohydrates in Chemistry and Biology*; Ernst, B., Hart, G. W., Sinay, P., Eds.; Wiley-VCH: Weinheim, Germany, 2000.

(17) Crich, D. Chemistry of Glycosyl Triflates: Synthesis of β-Mannopyranosides. *J. Carbohydr. Chem.* **2002**, *21*, 663–686.

(18) Demchenko, A. V. Stereoselective Chemical 1,2-cis O-Glycosylation: From 'Sugar Ray' to Modern Techniques of the 21st Century. *Synlett* **2003**, 1225–1240.

(19) Crich, D.; Chandrasekara, N. S. Mechanism of 4,6-O-Benzylidene-Directed β-Mannosylation as Determined by α-Deuterium Kinetic Isotope Effects. *Angew. Chem., Int. Ed.* **2004**, *43*, 5386–5389.

(20) Yamago, S.; Yamada, T.; Maruyama, T.; Yoshida, J. Iterative Glycosylation of 2-Deoxy-2-aminothioglycosides and Its Application to the Combinatorial Synthesis of Linear Oligoglucosamines. *Angew. Chem., Int. Ed.* **2004**, *43*, 2145–2148.

(21) Wei, P.; Kerns, R. J. Factors Affecting Stereocontrol during Glycosidation of 2,3-Oxazolidinone-Protected 1-Tolythio-N-acetyl-D-glucosamine. *J. Org. Chem.* **2005**, *70*, 4195–4198.

(22) Horenstein, N. A. Mechanisms for Nucleophilic Aliphatic Substitution at Glycosides. *Adv. Phys. Org. Chem.* **2006**, *41*, 275–314.

(23) Rencurosi, A.; Lay, L.; Russo, G.; Caneva, E.; Poletti, L. NMR Evidence for the Participation of Triflated Ionic Liquids in Glycosylation Reaction Mechanisms. *Carbohydr. Res.* **2006**, *341*, 903–908.

(24) Baek, J.-Y.; Choi, T. J.; Jeon, H.-B.; Kim, K.-S. A Highly Reactive and Stereoselective β-Mannopyranosylation System: Mannosyl 4-Pentenoate/PhSeOTf. *Angew. Chem., Int. Ed.* **2006**, *45*, 7436–7440.

(25) Lucero, C. G.; Woerpel, K. A. Stereoselective C-Glycosylation Reactions of Pyranoses: The Conformational Preference and Reactions of the Mannosyl Cation. *J. Org. Chem.* **2006**, *71*, 2641–2647.

(26) Smith, D. M.; Woerpel, K. A. Electrostatic Interactions in Cations and Their Importance in Biology and Chemistry. *Org. Biomol. Chem.* **2006**, *4*, 1195–1201.

(27) Jensen, H. H.; Bols, M. Stereoelectronic Substituent Effects. *Acc. Chem. Res.* **2006**, *39*, 259–265.

(28) Nokami, T.; Shibuya, A.; Tsuyama, H.; Suga, S.; Bowers, A. A.; Crich, D.; Yoshida, J. Electrochemical Generation of Glycosyl Triflate Pools. *J. Am. Chem. Soc.* **2007**, *129*, 10922–10928.

(29) Park, J.; Kawatkar, S.; Kim, J.-H.; Boons, G.-J. Stereoselective Glycosylations of 2-Azido-2-deoxy-glucosides Using Intermediate Sulfonium Ions. *Org. Lett.* **2007**, *9*, 1959–1962.

(30) Crich, D.; Sharma, I. Is Donor-Acceptor Hydrogen Bonding Necessary for 4,6-O-Benzylidene-directed β-Mannopyranosylation? Stereoselective Synthesis of β-C-Mannopyranosides and α-C-Glucopyranosides. *Org. Lett.* **2008**, *10*, 4731–4734.

(31) Manabe, S.; Ito, Y. Optimizing Glycosylation Reaction Selectivities by Protecting Group Manipulation. *Curr. Bioactive Compounds* **2008**, *4*, 258–281.

(32) Krumer, J. R.; Salamant, W. A.; Woerpel, K. A. Continuum of Mechanisms for Nucleophilic Substitutions of Cyclic Acetals. *Org. Lett.* **2008**, *10*, 4907–4910.

(33) Walvoot, M. T. C.; Lodder, G.; Mazurek, J.; Overkleeft, H. S.; Cdée, J. D. C.; van der Marel, G. A. Equatorial Anomeric Triflates from Mannuronic Acid Esters. *J. Am. Chem. Soc.* **2009**, *131*, 12080–12081.

(34) Zhu, X.; Schmidt, R. R. New Principles for Glycoside-Bond Formation. *Angew. Chem., Int. Ed.* **2009**, *48*, 1900–1934.

(35) Boltje, T. J.; Buskas, T.; Boons, G.-J. Opportunities and Challenges in Synthtic Oligosaccharide and Glycoconjugate Research. *Nature Chem.* **2009**, *1*, 611–622.

(36) Yang, M. T.; Woerpel, K. A. The Effect of Electrostatic Interactions on Conformational Equilibria of Multiply Substituted Tetrahydropyran Oxocarbenium Ions. *J. Org. Chem.* **2009**, *74*, 545–553.

(37) Krumper, J. R.; Salamant, W. A.; Woerpel, K. A. Correlations Between Nucleophilicities and Selectivities in the Substitutions of Tetrahydropyran Acetals. *J. Org. Chem.* **2009**, *74*, 8039–8050.

(38) Baek, J. Y.; Lee, B.-Y.; Jo, M. Gi.; Kim, K. S. β-Directing Effect of Electron-Withdrawing Groups at *O*-3, *O*-4, and *O*-6 Positions and α-Directing Effect by Remote Participation of 3-*O*-Acyl and 6-*O*-Acetyl Groups of Donors in Mannopyranosylations. *J. Am. Chem. Soc.* **2009**, *131*, 17705–17713.

(39) Stalford, S. A.; Kilner, C. A.; Leach, A. G.; Turnbull, W. B. Neighboring Group Participation vs. Addition to Oxacarbenium Ions: Studies on The Synthesis of Mycobacterial Oligosaccharides. *Org. Biomol. Chem.* **2009**, *7*, 4842–4852.

(40) Post, C. B.; Karplus, M. Does Lysozyme Follow the Lysozyme Pathway? An Alternative Based on Dynamic, Structural, and

Stereoelectronic Consideration. *J. Am. Chem. Soc.* **1986**, *108*, 1317–1319.

(41) Andrews, C. W.; Fraser-Raid, B.; Bowen, J. P. An ab Initio Study (6-31G*) of Transition States in Glycoside Hydrolysis Based on Axial and Equatorial 2-Methoxytetrahydropyrans. *J. Am. Chem. Soc.* **1991**, *113*, 8293–8298.

(42) Woods, R. J.; Andrews, C. W.; Bowen, J. P. Molecular Mechanical Investigations of the Properties of Oxocarbenium Ions. 2. Application to Glycoside Hydrolysis. *J. Am. Chem. Soc.* **1992**, *114*, 859–864.

(43) Andrew, C. W.; Rodebaugh, R.; Fraser-Raid, B. A Solvation-Assisted Model for Estimating Anomeric Reactivity. Predicted versus Observed Trends in Hydrolysis of n-Pentenyl Glycosides. *J. Org. Chem.* **1996**, *61*, 5280–5289.

(44) Bérces, A.; Enright, G.; Nukada, T.; Whitfield, D. M. The Conformational Origin of the Barrier to the Formation of Neighboring Group Assistance in Glycosylation Reactions: A Dynamical Density Functional Theory Study. *J. Am. Chem. Soc.* **2001**, *123*, 5460–5464.

(45) Bérces, A.; Whitfield, D. M.; Nukada, T. Quantitative Description of Six-Membered Ring Conformations Following the IUPAC Conformational Nomenclature. *Tetrahedron* **2001**, *57*, 477–491.

(46) Nukada, T.; Bérces, A.; Whitfield, D. M. Can The Stereochemical Outcome of Glycosylation Reactions Be Controlled by The Conformational Preferences of The Glycosyl Donor. *Carbohydr. Res.* **2002**, *337*, 765–774.

(47) Stubbs, J. M.; Marx, D. Glycosidic Bond Formation in Aquous Solution: On the Oxocarbenium Intermediate. *J. Am. Chem. Soc.* **2003**, *125*, 10960–10962.

(48) Bérces, A.; Whitfield, D. M.; Nukada, T.; do Santos, Z. I.; Obuchowska, A.; Krepinsky, J. J. Glycosylation: Is Acyl Migration to The Aglycon Avoidable in 2-Acyl Assisted Reactions. *Can. J. Chem.* **2004**, *82*, 1157–1171.

(49) Nukada, T.; Bérces, A.; Wang, L.; Zgierski, M. Z.; Whitfield, D. M. The Two-conformer Hypothesis: 2,3,4,6-tetra-O-methyl-mannopyranosyl And -glucopyranosyl Oxacarbenium Ions. *Carbohydr. Res.* **2005**, *340*, 841–852.

(50) Denekamp, C.; Sandlers, Y. Formation and Stability of Oxocarbenium Ions from Glycosides. *J. Mass Spectrom.* **2005**, *40*, 1055–1063.

(51) Stubbs, J. M.; Marx, D. Aspects of Glycosidic Bond Formation in Aquous Solution: Chemical Bonding and the Role of Water. *Chem.—Eur. J.* **2005**, *11*, 2651–2659.

(52) Ionescu, A. R.; Whitfield, D. M.; Zierskia, M. Z.; Nukada, T. Investigations into The Role of Oxacarbenium Ions in Glycosylation Reactions by ab Initio Molecular Dynamics. *Carbohydr. Res.* **2006**, *341*, 2912–2920.

(53) Whitfield, D. M.; Nukada, T. DFT Studies of The Role of C-2-O-2 Bond Rotation in Neighboring-group Glycosylation Reactions. *Carbohydr. Res.* **2007**, *342*, 1291–1304.

(54) Biarnés, X.; Ardèvol, A.; Planas, A.; Rovira, C.; Laio, A.; Parrinello, M. The Conformational Free Energy Landscape of β-D-Glucopyranose. Implications for Substrate Preactivation in β-Glucoside Hydrolases. *J. Am. Chem. Soc.* **2007**, *129*, 10686–10693.

(55) Whitfield, D. M. Computational Studies of the Role of Glycopyranosyl Oxacarbenium Ions in Glycobiology and Glycochemistry. *Adv. Carbohydr. Chem. Biochem.* **2009**, *62*, 83–159.

(56) Codée, J. D. C.; van den Bos, L. J.; de Jong, A.-R.; Dinkelaar, J.; Lodder, G.; Overkleeft, H. S.; van der Marel, G. A. The Stereodirecting Effect of the Glycosyl C5-Carboxylate Ester: Stereoselective Synthesis of β-Mannuronic Acid Alginates. *J. Org. Chem.* **2009**, *74*, 38–47.

(57) Pougny, J.-R.; Sinaÿ, P. Reaction d'imidates de glucoyranosyle avec l'acetonitrile. Applications synthetiques. *Tetrahedron Lett.* **1976**, *17*, 4073–4076.

(58) Lemieux, R. U.; Ratcliffe, R. M. The Azidonitration of Tri-*O*-acetyl-D-galactal. *Can. J. Chem.* **1979**, *57*, 1244–1251.

(59) Schmidt, R. R.; Rücker, E. Stereoselective Glycosidations of Uronic Acids. *Tetrahedron Lett.* **1980**, *21*, 1421–1424.

(60) Paulsen, H. Advances in Selective Chemical Syntheses of Complex Oligosaccharides. *Angew. Chem., Int. Ed.* **1982**, *21*, 155–173.

(61) Hashimoto, S.; Hayashi, M.; Noyori, R. Glycosylation Using Glucopyranosyl Fluorides And Silicon-based Catalysts. Solvent Dependency of the Stereoselection. *Tetrahedron Lett.* **1984**, *25*, 1379–1382.

(62) Braccini, I.; Derouet, C.; Esnault, J.; Herve du Penhoat, C.; Mallet, J.-M.; Michon, V.; Sinaÿ, P. Conformational Analysis of Nitrilium Intermediates in Glycosylation Reactions. *Carbohydr. Res.* **1993**, *246*, 23–41.

(63) Uchiro, H.; Mukaiyama, T. Trityl Salt Catalyzed Sterelective Glycosylation of Alcohols with 1-Hydroxyribofuranose. *Chem. Lett.* **1996**, *1*, 79–80.

(64) Demchenko, A.; Stauch, T.; Boons, G. J. Solvent and Other Effects on the Stereoselectivity of Thioglycoside Glycosidations. *Synlett* **1997**, 818–820.

(65) Manabe, S.; Ito, Y.; Ogawa, T. Solvent Effect in Glycosylation Reaction on Polymer Support. *Synlett* **1998**, 628–630.

(66) Rencurosi, A.; Lay, L.; Russo, G.; Caneva, E.; Poletti, L. Glycosylation with Trichloroacetimidates in Ionic Liquids: Influence of the Reaction Medium on the Stereochemical Outcome. *J. Org. Chem.* **2005**, *70*, 7765–7768.

(67) Koshiba, M.; Suzuki, N.; Arihara, R.; Tsuda, T.; Nambu, H.; Nakamura, S.; Hashimoto, S. Catalytic Stereoselective Glycosidation with Glycosyl Diphenyl Phosphates: Rapid Construction of 1,2-*cis*-α-Glycosidic Linkages. *Chem. Asian J.* **2008**, *3*, 1664–1677.

(68) Whitfield, D. M. DFT Studies of the Ionization of Alpha and Beta Glycopyranosyl Donors. *Carbohydr. Res.* **2007**, *342*, 1726–1740.

(69) Becke, A. D. Density-functional thermochemistry. III. The role of exact exchange. *J. Chem. Phys.* **1993**, *98*, 5648–5652.

(70) Stephens, P. J.; Devlin, F. J.; Chabalowski, C. F.; Frisch, M. J. Ab Initio Calculation of Vibrational Absorption and Circular Dichroism Spectra Using Density Functional Force Fields. *J. Phys. Chem.* **1994**, *98*, 11623–11627.

(71) Frisch, M. J.; Trucks, G. W.; Schlegel, H. B.; Scuseria, G. E.; Robb, M. A.; Cheeseman, J. R.; Montgomery, J. A., Jr.; Vreven, T.; Kudin, K. N.; Burant, J. C.; Millam, J. M.; Iyengar, S. S.; Tomasi, J.; Barone, V.; Mennucci, B.; Cossi, M.; Scalmani, G.; Rega, N.; Petersson, G. A.; Nakatsuji, H.; Hada, M.; Ehara, M.; Toyota, K.; Fukuda, R.; Hasegawa, J.; Ishida, M.; Nakajima, T.; Honda, Y.; Kitao, O.; Nakai, H.; Klene, M.; Li, X.; Knox, J. E.; Hratchian, H. P.; Cross, J. B.; Bakken, V.; Adamo, C.; Jaramillo, J.; Gomperts, R.; Stratmann, R. E.; Yazyev, O.; Austin, A. J.; Cammi, R.; Pomelli, C.; Ochterski, J. W.; Ayala, P. Y.; Morokuma, K.; Voth, G. A.; Salvador, P.; Dannenberg, J. J.; Zakrzewski,

V. G.; Dapprich, S.; Daniels, A. D.; Strain, M. C.; Farkas, O.; Malick, D. K.; Rabuck, A. D.; Raghavachari, K.; Foresman, J. B.; Ortiz, J. V.; Cui, Q.; Baboul, A. G.; Clifford, S.; Cioslowski, J.; Stefanov, B. B.; Liu, G.; Liashenko, A.; Piskorz, P.; Komaromi, I.; Martin, R. L.; Fox, D. J.; Keith, T.; Al-Laham, M. A.; Peng, C. Y.; Nanayakkara, A.; Challacombe, M.; Gill, P. M. W.; Johnson, B.; Chen, W.; Wong, M. W.; Gonzalez, C.; Pople, J. A. *Gaussian 03*, Revision C.02; Gaussian, Inc., Wallingford CT, 2004.

(72) Tomasi, J.; Mennucci, B.; Cammi, R. Quantum Mechanical Continuum Solvation Models. *Chem. Rev.* **2005**, *105*, 2999–3093.

(73) Lemieux, R. U. Effects of Unshared Pairs of Electrons and Their Solvation on Conformational Equilibria. *Pure Appl. Chem.* **1971**, *25*, 527–548.

(74) *Gauss View*, version 3.0.; Gaussian, Inc.: Pittsburgh, PA, 2003.

(75) Christen, M.; Hünenberger, P. H.; Bakowies, D.; Baron, R.; Bürgi, R.; Geerke, D. P.; Heinz, T. N.; Kastenholz, M. A.; Kräutler, V.; Oostenbrink, C.; Peter, C.; Tryesniak, D.; van Gunsteren, W. F. The GROMOS Software for Biomolecular Simulation: GROMOS05. *J. Comput. Chem.* **2005**, *26*, 1719–1751.

(76) Oostenbrink, C.; Villa, A.; Mark, A. E.; van Gunsteren, W. F. A Biomolecular Force Field Based on the Free Enghalpy of Hydration and Solvation: The GROMOS Force-Field Parameter Sets 53A5 and 53A6. *J. Comput. Chem.* **2004**, *25*, 1656–1676.

(77) Oostenbrink, C.; Soares, T. A.; van der Vegt, N. F. A.; van Gunsteren, W. F. Validation of the 53A6 GROMOS Force Field. *Eur. Biophys. J.* **2005**, *34*, 273–284.

(78) Lins, R. D.; Hünenberger, P. H. A New GROMOS Force Field for Hexopyranose-Based Carbohydrates. *J. Comput. Chem.* **2005**, *26*, 1400–1412.

(79) Pereira, C. S.; Kony, D.; Baron, R.; Müller, M.; van Gunsteren, W. F.; Hünenberger, P. H. Conformational and Dynamical Properties of Disaccharides in Water: A Molecular Dynamics Study. *Biophys. J.* **2006**, *90*, 4337–4344.

(80) Pereira, C. S.; Kony, D.; Baron, R.; Müller, M.; van Gunsteren, W. F.; Hünenberger, P. H. Erratum to "Conformational and dynamical properties of disaccharides in water: A molecular dynamics study. *Biophys. J.* **2007**, *93*, 706–707.

(81) Kräutler, V.; Müller, M.; Hünenberger, P. H. Conformation, Dynamics, Solvation and Relative Stabilities of Selected β-Hexopyranoses in Water: A Molecular Dynamics Study with the GROMOS 45A4 Force Field. *Carbohydr. Res.* **2007**, *342*, 2097–2124.

(82) Hansen, H. S.; Hünenberger, P. H. Using the Local Elevation Method to Construct Optimized Umbrella Sampling Potentials: Calculation of the Relative Free Energies and Interconversion Barriers of Glucopyranose Ring Conformers in Water. *J. Comput. Chem.* **2010**, *31*, 1–23.

(83) *The Merck Index*, 13th ed.; Merck & Co., Inc.: Whitehouse Station, NJ.

(84) Berendsen, H. J. C.; Postma, J. P. M.; van Gunsteren, W. F.; Di Nola, A.; Haak, J. R. Molecular Dynamics with Coupling to an External Bath. *J. Chem. Phys.* **1984**, *81*, 3684–3690.

(85) Ryckaert, J.-P.; Ciccotti, G.; Berendsen, H. J. C. Numerical Integration of the Cartesian Equations of Motion of a System with Constraints: Molecular Dynamics of *n*-Alkanes. *J. Comput. Phys.* **1977**, *23*, 327–341.

(86) van Gunsteren, W. F.; Berendsen, H. J. C. Computer Simulation of Molecular Dynamics: Methodology, Applications and Perspectives in Chemistry. *Angew. Chem., Int. Ed.* **1990**, *29*, 992–1023.

(87) Sigma-Aldrich. http://www.sigmaaldrich.com/chemistry/solvents/toluene-center.html (accessed April 13, 2010).

(88) Yasumi, M.; Shirai, M. The Dielectric Constant of 1,4-Dioxane. *Bull. Chem. Soc. Jpn.* **1955**, *28*, 193–196.

(89) Rao, V. S. R.; Qasba, P. K.; Balaji, P. V.; Chandrasekaran, R. *Conformation of Carbohydrates*; Harwood Academic Publishers: Amsterdam, The Netherlands, 1998.

(90) Romero, J. A. C.; Tabacco, S. A.; Woerpel, K. A. Stereochemical Reversal of Nucleophilic Substitution Reactions Depending upon Substituent: Reactions of Heteroatoms-Substituted Six-Memberd-Ring Oxocarbenium Ions through Pseudoaxial Conformers. *J. Am. Chem. Soc.* **2000**, *122*, 168–169.

(91) Ionescu, A.; Wang, L.; Zgierski, M. Z.; Nukada, T.; Whitfield, D. M. Two Unexpected Effects Found with 2,3,4,6-Tetra-O-methyl-D-Gluco- and Mannopyranosyl Oxacarbenium Ions. In *NMR Spectroscopy and Computer Modeling of Carbohydrates*; Vliegenthar, H., Woods, R. J., Eds.; *Am. Chem. Soc. Symp. Ser.*, 2006, *930*, 302−319.

(92) Ayala, L.; Lucero, C. G.; Romero, J. A. C.; Tabacco, S. A.; Woerpel, K. A. Stereochemistry of Nucleophilic Substitution Reactions Depending upon Substituent: Evidence for Electrostatic Stabilization of Pseudoaxial Conformers of Oxocarbenium Ions by Heteroatoms Substituents. *J. Am. Chem. Soc.* **2003**, *125*, 15521–15528.

(93) Crich, D.; Vinod, A. U. Oxazolidinone Protection of *N*-Acetylglucosamine Confers High Reactivity on the 4-Hydroxy Group in Glycosylation. *Org. Lett.* **2003**, *5*, 1297–1300.

(94) Crich, D.; Vinod, A. U. 6-*O*-Silyl-*N*-acetyl-2-amino-2-*N*,3-*O*-carbonyl-2-deoxyglucosides: Effective Glycosyl Acceptors in the Glucosamine 4-OH Series. Effect of Anomeric Stereochemistry on the Removal of the Oxazolidinone Group. *J. Org. Chem.* **2005**, *70*, 1291–1296.

(95) Manabe, S.; Ishii, K.; Ito, Y. N-Benzyl-2,3-oxazolidinone as a Glycosyl Donor for Selective α-Glycosylation and One-Pot Oligosaccharide Synthesis Involving 1,2-*cis*-Glycosylation. *J. Am. Chem. Soc.* **2006**, *128*, 10666–10667.

(96) Crich, D.; Cai, F.; Yang, F. A Stable, Commercially Available Sulfenyl Chloride for the Activation of Thioglycosides in Conjunction with Silver Trifluoromethanesulfonate. *Carbohydr. Res.* **2008**, *343*, 1858–1862.

(97) Lemieux, R. U. Newer Developments in the Conformational Analysis of Carbohydrates. *Pure Appl. Chem.* **1971**, *25*, 527–547.

(98) Lemieux, R. U.; Hendriks, K. B.; Stick, R. V.; James, K. Halide Ion Catalyzed Glycosidation Reactions. Syntheses of α-Linked Disaccharides. *J. Am. Chem. Soc.* **1975**, *97*, 4056–4062.

CT1001347